Journal of Power Sources 509 (2021) 230367

Contents lists available at ScienceDirect

Journal of Power Sources

journal homepage: www.elsevier.com/locate/jpowsour

Storage batteries in photovoltaic–electrochemical device for solar hydrogen production

O. Astakhov *, S.N. Agbo, K. Welter, V. Smirnov, U. Rau, T. Merdzhanova

Institute of Energy and Climate Research (IEK-5)-Photovoltaics, Forschungszentrum Jülich GmbH, 52428, Jülich, Germany

HIGHLIGHTS

- Battery cell implemented in photovoltaic-assisted water splitting device.
- Feasibility of continuous water splitting without power electronics.
- Spreading of light energy over diurnal cycle reduces overpotential in water splitting.
- Improved solar-to-hydrogen efficiency despite battery losses.

ARTICLE INFO

Keywords:
Battery implemented in cell-to-cell photovoltaic assisted water splitting system
Continuous water splitting
Unaided water splitting
Reduction of overpotential loss
Improved solar-to-hydrogen efficiency

ABSTRACT

Hydrogen produced by water electrolysis, and electrochemical batteries are widely considered as primary routes for the long- and short-term storage of photovoltaic (PV) energy. At the same time fast power ramps and idle periods in PV power generation may cause degradation of water splitting electrochemical (EC) cells. Implementation of batteries in PV-EC systems is a viable option for smoothening out intermittence of PV power. Notably, the spreading of PV energy over the diurnal cycle reduces power of the EC cell and thus its overpotential loss. We study these potential advantages theoretically and experimentally for a simple parallel connected combination of PV, EC, and battery cells (PV-EC-B) operated without power management electronics. We show feasibility of the unaided operation of PV-EC-B device in a relevant duty cycle and explore how PV-EC-B system can operate at higher solar-to-hydrogen efficiency than the equivalent reference PV-EC system despite the losses caused by the battery.

1. Introduction

According to the "Global energy system based on 100% renewable energy" report [1], Photovoltaics (PV) is expected to cover 69% of total primary energy generation in the global renewable energy system in the future. This will require large amount of storage to stabilize power supply. It is expected that short term storage of PV energy will be covered by electrochemical batteries, and long term storage by solar fuels, such as hydrogen produced by water electrolysis [1]. Combinations of PV devices with electrochemical (EC) cells for water splitting [2–12] or with batteries (B) [13–19] have been widely addressed in the literature. It has been found in particular, that intermittent nature of PV power generation with fast power ramps and idle periods cause degradation of water electrolyzers [20]. Implementation of batteries in PV-electrolyzer systems is beneficial to smoothen PV power fluctuation and stabilize performance of the EC components as demonstrated on residential PV system scale [21]. In our previous works we addressed integration of PV cells with EC water splitting cells (PV-EC) [8,11,22] as well as PV-battery integration (PV–B) [23–26] at cell-to-cell level. In both cases PV cells are directly integrated/connected to an EC or a battery. In this work we investigate behavior and performance of a system with a PV cell directly coupled to an EC cell and a battery (PV-EC-B device). All elements are connected in parallel without power management electronics to address most material saving solution. Thus, this combination can be considered as a basic unit of a PV-driven power source with both short-term and long-term energy storage functions. Such minimalistic combination of PV, battery and water splitting devices can hypothetically function without the need for power management electronics, smoothing out irradiance instabilities and maintaining stable hydrogen generation in a soft regime. The study addresses two main questions:

* Corresponding author.
E-mail address: o.astakhov@fz-juelich.de (O. Astakhov).

https://doi.org/10.1016/j.jpowsour.2021.230367
Received 18 June 2021; Received in revised form 30 July 2021; Accepted 7 August 2021
Available online 19 August 2021

Glossary

PV	photovoltaic cell or module
EC	electrochemical cell
B	battery
PV-EC	combined device with PV directly connected to EC
PV-EC-B	combined device with PV directly connected in parallel to EC and B
STH	solar-to-hydrogen efficiency of PV-EC system
*STH**	solar-to-hydrogen efficiency of PV-EC-B system calculated under specific conditions
ΔSTH	difference of STH between PV-EC and PV-EC-B systems (*STH**-*STH*)
T_l	duration of the light period in the duty cycle
T_d	duration of the dark period during the duty cycle so that T_d[h] + T_l [h] = 24 h
I_{PV}	PV current
I_{ECl}	EC cell current during T_l
I_{Bl}	battery current during T_l (battery charging current)
I_{ECd}	EC cell current during T_d and at the same time a battery discharge current I_{Bd}
I_{WP}	working point current
I_{MPP}	maximum power point (MPP) current
V_{WP}	working point voltage
V_{MPP}	maximum power point voltage
V_{OCB}	battery open circuit voltage
V_{EC}	EC cell voltage
V_{ECl}	EC cell voltage during T_l
V_{ECd}	EC cell voltage during T_d
V_{opEC}	EC cell overpotential with respect to is the thermodynamic potential of water electrolysis (ΔE = 1.23 V at 25 °C)
V_{opl}	EC cell overpotential during T_l with respect to ΔE = 1.23 V
V_{opd}	EC cell overpotential during T_d with respect to ΔE = 1.23 V
V_{opB}	roundtrip overpotential in a battery the difference of charge and discharge voltages
Q_{H2}	electric charge utilized in water splitting process
Q_{H2l}	electric charge utilized in water splitting process during T_l
Q_{H2d}	electric charge utilized in water splitting process during T_d
Q_B	electric charge stored in a battery during T_l
P_{in}	total power of light arriving at PV device
P_{ECl}	power consumed by an EC cell during T_l
P_{Bl}	power of a battery charging during T_l
P_{H2l}	power delivered to hydrogen during T_l
P_{H2d}	power delivered to hydrogen during T_d
P_{MPP}	maximum power of a PV device under fixed irradiance
P_{WP}	power of a PV device at a given working point (WP)
MPP	maximum power point of a PV device
η	efficiency of a PV device
η_{FB}	Faradaic efficiency of a battery
η_{FEC}	Faradaic efficiency of an EC cell
ΔE	thermodynamic potential of water electrolysis (ΔE = 1.23 V at 25 °C)
C	coupling factor, the ratio working point power to the maximum power of a PV device P_{WP}/P_{MPP}
IV	current-voltage characteristics of PV, EC, or battery

Is it possible to drive water splitting unaided over a realistic duty cycle for a system of parallel connected PV, EC and battery cells?

How does the implementation of the battery affect solar-to-hydrogen efficiency in PV-EC-B system in comparison to the reference PV-EC system?

First, we address both questions theoretically to identify fundamental difference between PV-EC-B and PV-EC systems. We consider the basic system structure, interaction of current-voltage (IV) characteristics of system components and effect of the battery on PV working point, power coupling and potential losses [27]. Next, simple duty cycle of light and dark periods and charge balance in PV-EC-B system is addressed. Finally, we provide formulation to estimate solar-to-hydrogen (STH) efficiency convenient for direct comparison of both PV-EC-B and PV-EC systems using available IV characteristics. We show that the simple PV-EC-B system not only can provide required behavior in diurnal cycle, but potentially can outperform reference PV-EC system.

Feasibility of the unaided operation of parallel connected PV-EC-B system is demonstrated experimentally with a multijunction thin film PV cell [8,28] connected to an EC cell with simple Ni/Ni catalyst system [11], and Li-ion battery cell [29,30].

Finally, we combine the experimental IVs of the PV and EC cells with simple battery simulations [26] to explore optimization directions for the PV-EC-B system with emphasis on the battery voltage. Effect of battery voltage is studied first using the experimentally measured system and next, we explore potential STH gain in this system with optimal power coupling and high battery capacity.

2. Theoretical analysis of the PV-EC-B system

2.1. PV-EC-B system

The role of the battery in the PV-EC-B system, is analyzed in comparison with the well understood reference PV-EC system [11,31,32]. We assume that both systems operate in natural periodic day-night cycle. Fig. 1 (a) shows power flow diagram of the PV-EC-B system. The key difference to a typical PV-EC system [2–7,9–12] is the splitting of PV power into power of electrochemical cell (P_{ECl}) and power of the battery (P_{Bl}) during the light period shown with red arrows in Fig. 1 (a). The energy stored in the battery during light period can be delivered to the EC cell in the dark (blue arrow P_{ECd} in Fig. 1 (a)).

The PV energy therefore can be delivered to hydrogen with P_{H2l} during light and P_{H2d} during dark periods of the duty cycle. We consider simple realization of the PV-EC-B concept with parallel connected EC and battery cells to a PV cell as presented in Fig. 1 (b). In this PV-EC-B system the PV cell current I_{PV} is split unaided into the light current of the EC cell (I_{ECl}) and light battery current (I_{Bl}) while EC and battery voltages are equal to the PV voltage. As the light period is over the PV cell is off and the battery drives the EC cell with stored energy. In this case the dark battery current I_{Bd} is only flowing to the EC cell so that the dark EC current $I_{ECd} = I_{Bd}$. Voltages of both battery and EC cell are equal. For the sake of brevity, whenever possible we use expressions like “light EC current” or “light battery current” for the parameters related to light and dark operation modes.

2.2. IV characteristics and power coupling

In order to understand the effect of connecting a battery to a PV-EC system we consider a set of typical IV-characteristics relevant for both PV-EC and PV-EC-B systems. Sample current-voltage characteristics of a PV cell, an EC cell, and a battery are presented in Fig. 2. In the case of directly connected PV-EC combination the working point of the system is at the intersection of PV and EC IV characteristics. Note that working point of the PV-EC system does not coincide with the maximum power point of the PV cell (MPP in Fig. 2) which is the general case. This means that PV cell output power is below the attainable maximum, and the overall solar-to-hydrogen efficiency [27] is reduced.

This loss referred to as “coupling loss” [27] can be minimized with

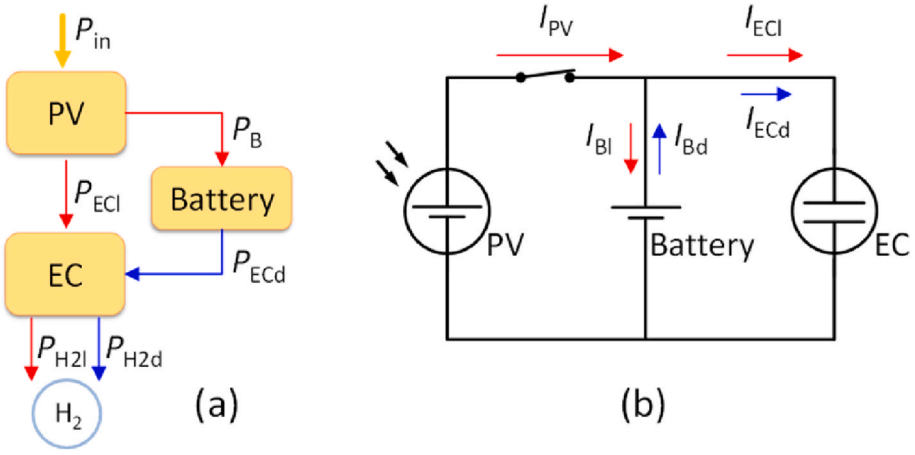

Fig. 1. (a) Power flow diagram of the PV-EC-B system. Power flow under irradiance is indicated with red arrows and blue arrows indicate power flow in the dark. (b) Circuit diagram of the PV-EC-B device. Red arrows indicate currents under sufficient irradiance: I_{PV} – current of the solar cell, I_{ECl} – current through the EC cell, I_{Bl} – current through the battery (charging current). Blue arrows indicate current in dark conditions when the solar cell is disconnected: I_{Bd} is the discharge current of the battery flowing to the EC cell only plainly equal to the current of the EC cell $I_{ECd} = I_{Bd}$. (For interpretation of the references to color in this figure legend, the reader is referred to the Web version of this article.)

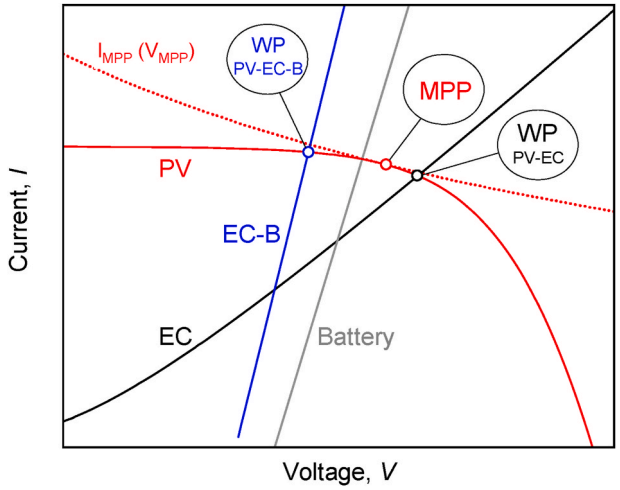

Fig. 2. An example set of IV characteristics of a PV cell (PV), electrochemical cell (EC), battery (B), and the EC-B combination (EC-B) for the light period. The scale is magnified to represent most relevant part of the IV characteristics. Three characteristic points are indicated: maximum power point of the PV cell (MPP), working point of the PV-EC system (WP PV-EC), and working point of the PV-EC-B system (WP PV-EC-B). Red dotted line "PV MPP" represents the dependence I_{MPP} (V_{MPP}) at η_{PV} = const and P_{in} = const – the set of maximum power points for variety of PV devices of same area and efficiency. (For interpretation of the references to color in this figure legend, the reader is referred to the Web version of this article.)

preselection of PV and EC parameters [8,33,34] or by employing maximum power point trackers (MPPT) [35] (the latter is out of consideration in our work). The degree of power coupling can be quantified with a coupling factor C – a ratio of working point power P_{WP} to the maximum power P_{MPP} of a PV cell or module:

$$C = \frac{P_{WP}}{P_{MPP}} = \frac{I_{WP}V_{WP}}{I_{MPP}V_{MPP}} \quad (1)$$

where I_{WP} and V_{WP} are current and voltage of working point, I_{MPP} and V_{MPP} are current and voltage of the maximum power point of the PV device. Coupling factor is unity when WP coincides with MPP – condition of optimal power matching when the maximum attainable PV power is utilized. The effect of the coupling factor on the solar to hydrogen efficiency of a PV-EC system can be formulated using efficiencies of the PV device (η_{PV}) and the EC device (η_{EC}) as follows:

$$STH = \eta_{PV} C \eta_{EC} \quad (2)$$

where η_{EC} is the DC-power-to-hydrogen efficiency of an EC cell. It is apparent that coupling factor has to be taken into account when comparing different PV water splitting systems, to separate effects related to the efficiency of components like η_{PV} or η_{EC}, from the effects related to their mutual power coupling.

In the case of PV-EC-B system the PV cell is connected in parallel to EC and battery (Fig. 1. (b)). The sum of EC and battery currents will result in common EC-B current. In Fig. 2 the sum of grey battery IV with the black EC IV results in common blue EC-B IV. The working point of the PV-EC-B system is at the intersection of PV and EC-B characteristics as shown in Fig. 2. The working point of PV-EC-B system is shifted to lower voltage with respect to the PV-EC system having same PV and EC cells. Two key aspects are to underline here: (i) the *battery can shift working point in PV-EC-B system* as compared to PV-EC combination affecting power coupling; and (ii) *this shift is towards lower working point voltage*. The latter point is of high relevance for the solar-to-hydrogen efficiency and will be discussed in detail in the next subsection, while we begin with the treatment of power coupling aspect. We can see that *battery can improve coupling in otherwise mismatched PV-EC system*, which is a particular case of matching PV to a load with aid of a battery [26]. Note that position of the battery IV on the voltage scale is generally not constant because battery open circuit voltage depends on its state of charge. In order to focus on the key difference between PV-EC and PV-EC-B systems we keep the position of the battery IV fixed as modern batteries in many cases exhibit flat charge/discharge characteristic [40–43]. Even though the influence of the battery can improve power coupling, this influence complicates comparison of PV-EC and PV-EC-B systems. One way to eliminate the shift of coupling is to use two different PV cells of same efficiency, but with different pairs of I_{MPP}-V_{MPP}, so that one cell is optimally matched to the EC cell and another one to the EC-B combination. In both cases then coupling factor is unity, $C = 1$, and thus can be taken out of consideration. These points of optimal coupling can be found graphically as shown in Fig. 2. Red dotted line in Fig. 2 represents the dependence of I_{MPP} on V_{MPP} for a range of possible PV devices with same PV efficiency, aperture, and test conditions, calculated according to:

$$I_{MPP}(V_{MPP}) = \frac{\eta_{PV} P_{in}}{V_{MPP}} \quad (3)$$

as reported in Ref. [10]. Intersections of the dotted line I_{MPP} (V_{MPP}) with IV characteristic of the EC cell or the EC-B combination in Fig. 2 give pairs of I_{MPP} and V_{MPP} for optimal coupling to two PV cells of same efficiency. In this way optimal coupling can be provided in both PV-EC and PV-EC-B systems and their efficiencies can be compared directly. In practice, appropriate pairs of solar cells may be at disposal, or alternatively, matching loss can be minimized with MPPT [35]. However, in

many cases two solar cells with the required maximum power points are challenging to access. In the experimental part of this work we used one and the same available solar cell. We compare the same PV-EC pair with and without battery to show practical feasibility of unaided PV-EC-B operation. Fundamental difference in efficiency between PV-EC and PV-EC-B systems with optimal coupling is addressed with simulations.

2.3. Potential losses and discharge phase

In this subsection we analyze theoretically (i) how feasible is the charge-discharge function in unaided, directly connected PV-EC-B combination; and (ii) how the shift of working point and battery overpotentials influence total potential losses (kinetic losses [27]) in PV-EC-B system compared to PV-EC reference. We start with plot of all relevant IV characteristics in Fig. 3.

Characteristic optimal coupling working points are numbered: 1 – working point of the PV-EC combination, 2 – working point of the PV-EC-B combination during light period, 3 – working point of the PV-EC-B combination during dark period.

The figure is divided in two parts: top part, Fig. 3 (a), the positive current hemispace for the light period T_l; and bottom part, Fig. 3 (b), the negative current hemispace for the dark period T_d. First, consider the light operation in Fig. 3 (a), where simulated IV characteristics of EC, battery, and EC-B combination are presented (both use the same EC cell). Note that no particular IV characteristics of the PV cell is considered. Instead we plot the dependence $I_{MPP}(V_{MPP})$ and find points of optimal coupling of EC and EC-B to two equivalent PV cells as described in the previous subsection.

In Fig. 3 (a) the intersection of the red dotted curve $I_{MPP}(V_{MPP})$ with black IV characteristics gives working point of optimal coupling for PV-EC system, marked "1". In the same way intersection between red dotted $I_{MPP}(V_{MPP})$ curve and blue IV characteristic of EC-B combination gives optimal working point for PV-EC-B system marked "2". It is obvious in Fig. 3 (a) that the blue EC-B curve is steeper than the black characteristics of the EC cell due to the summation EC and battery currents. Therefore, optimal working point "2" of PV-EC-B system is shifted to lower voltage and higher current as compared to the working point "1"

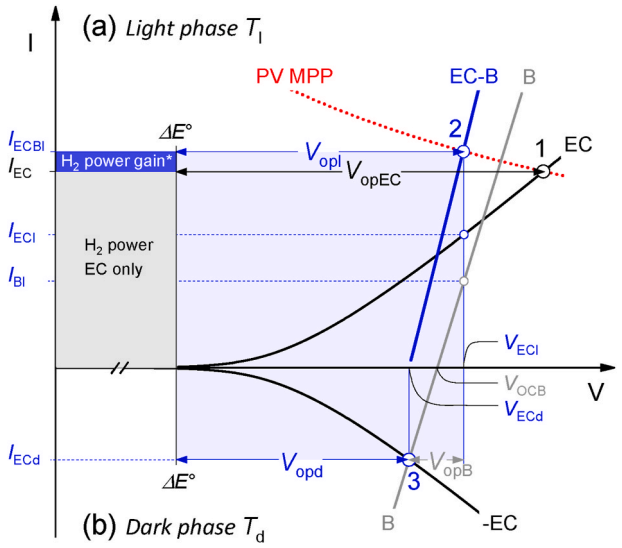

Fig. 3. (a) An example set of IV characteristics of electrochemical cell (EC), battery (B), and the EC-B combination (EC-B) for the light period T_l. Red line "PV MPP" represents the dependence $I_{MPP}(V_{MPP})$ – the set of maximum power points for variety of PV devices of same area and efficiency under same irradiation. (b) IV of the same battery (B) and flipped IV of the electrochemical cell (EC) representing the dark period T_d, when EC is driven by the battery. (For interpretation of the references to color in this figure legend, the reader is referred to the Web version of this article.)

of the EC-cell alone. Hence, during the light phase T_l the PV-EC-B system operates at *lower overpotential*, (see $V_{opl} < V_{opEC}$ in Fig. 3 (a)) and at *higher total current* ($I_{ECBl} > I_{EC}$) compared to the PV-EC reference, which is potentially beneficial for the solar-to-hydrogen efficiency. This reduction of overpotential is possible because actual light EC current I_{ECl} in PV-EC-B system is lower than I_{EC} in the reference PV-EC system, due to current splitting between EC and battery. It can be said therefore that *the inclusion of a battery into PV-EC system results in more efficient operation of EC cell owing to reduction of its operating current.* Whether or not this can boost total solar-to-hydrogen efficiency depends on the dark period performance of the PV-EC-B system.

The dark phase of PV-EC-B system operation is presented in Fig. 3 (b) extending the plot to the negative current hemispace. In Fig. 3 (b) the PV cell is idle and disconnected, the battery current is reversed, and the IV characteristic of the EC cell is flipped for consistency. Dark working point of the system is at the intersection of battery and EC characteristics indicated as "3" in Fig. 3 (b). It can be seen that significant current can be delivered to the EC cell from the battery in unaided operation. The whole Fig. 3 supports feasibility of unaided operation of PV-EC-B system with significant charging of the battery in the light phase, and discharging through the EC cell in the dark.

In order to address efficiency of this PV-EC-B operation we have to consider the potential losses arising during charge and discharge of the battery [36,37]. In Fig. 3 (b) total battery potential loss V_{opB} determines the voltage offset between light and dark working points "2" and "3". Considering the whole PV-EC-B system operation cycle, highlighted with a pale blue rectangle in Fig. 3, it can be seen that the light EC overpotential equals to the sum of EC and battery overpotentials in the dark:

$$V_{opl} = V_{opd} + V_{opB} = V_{ECl} - \Delta E^\circ \quad (4)$$

In other words, *both routes of current, direct PV-to-EC, and indirect PV-to-battery-to-EC, have same overpotential in PV-EC-B system*. The potential losses in the battery are compensated by the reduced dark overpotential of the EC cell. Equality (4) is a result of the fact that the initial potential V_{ECl} and final potential ΔE° are same for both paths, as long as the charge carriers leaving PV cell are utilized in the EC cell for water splitting. Notably in both light and dark operation phases the EC cell in PV-EC-B system operates at lower overpotential compared to the PV-EC reference (see Fig. 3). Since both total dark and light overpotentials are equal, there is no need to analyze the battery overpotential explicitly. Analysis of voltage efficiency in PV-EC-B system can be reduced to a consideration of the light working point "2" in Fig. 3 (a). Provided the charge stored in the battery is fully utilized, total current I_{ECBl} can be treated as a single current flowing to the EC cell. Under this condition, PV-EC-B system can be treated as an equivalent PV-EC system, which simplifies comparison to the PV-EC reference. The key charge utilization aspect is discussed in the next subsection.

2.4. Charge balance in PV-EC-B system

Performance of the PV-EC-B system strongly depends on the battery charge utilization in periodic operation. For simplicity, we consider a single "natural" duty cycle as two periods designated as light period T_l and dark period T_d so that $T_l + T_d = 24$ h. This simplification is based on the so called "Peak-Sun Hour" approach [38]. The duty cycle with relevant currents and charges is sketched in Fig. 4.

During the light period T_l, the PV current I_{PV} is divided into the light currents of EC I_{ECl}, and battery I_{Bl}. The battery light current I_{Bl} is shown negative to distinguish the charge stored in the battery Q_B from the charge utilized in the EC cell directly Q_{H2l}. During the dark period T_d, the battery charge Q_B is transferred to the EC cell with dark current I_{ECd}. Full charge utilization within one cycle of operation implies that $Q_{H2d} = Q_B$. A PV-EC-B system may deviate from $Q_{H2d} = Q_B$ condition when e.g. battery Faradaic efficiency η_{FB} is below 100%, but more importantly,

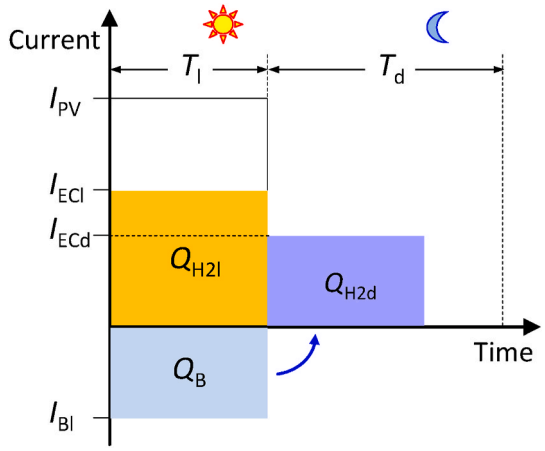

Fig. 4. Schematic presentation of currents and charges in a PV-EC-B system in a simplified duty cycle. Areas of colored rectangles represent total charge transferred through each element. The PV current I_{PV} is divided between EC and B (I_{ECl} and I_{Bl}) during T_l. During T_d the charge stored in the battery is delivered to EC at I_{ECd}.

when the product of the discharge current I_{ECd} and dark time T_d is insufficient to utilize the whole stored charge, so that $Q_B > I_{ECd}T_d$. Total charge delivered to the EC cell (Q_{H2}) can be expressed with charge utilization condition as follows:

$$Q_{H2} = \begin{cases} Q_{H2l} + \eta_{FB}Q_B\ ,\ Q_B < I_{ECd}T_d \\ Q_{H2l} + \eta_{FB}I_{ECd}T_d,\ Q_B > I_{ECd}T_d \end{cases} \quad (5)$$

Provided $Q_B < I_{ECd}T_d$ the PV-generated charge Q_{PV} is delivered to an EC cell except for eventual charge loss in a battery. Considering very high Faradaic (Coulombic) efficiencies achieved by modern batteries, $\eta_{FB} > 99\%$ [37], the charge utilization in the optimally operating PV-EC-B can be as good as in a simple PV-EC system. This regime can be referred to as "full charge utilization mode". The opposite situation $Q_B > I_{ECd}T_d$ can be described as "charge accumulation mode", when some charge will be transferred to the next cycle of operation. For the sake of clarity, we focus on the single duty cycle where full charge utilization is required to avoid losses. Both dark discharge current I_{ECd} and dark period T_d determine the charge utilization regime in the PV-EC-B system. Higher discharge current for longer time increases charge utilization and vice versa. The discharge current is in turn determined by the interplay of the EC and battery IVs as can be seen in Fig. 3 (b). The steeper the battery IV the closer is the dark discharge current I_{ECd} to the achievable maximum. The slope of the battery IV can be controlled in practice via the battery capacity. The time of discharge is usually determined by the natural duty cycle subject to geography and climate. In the section dedicated to the system limits and optimization we consider both battery capacity and discharge time.

2.5. Solar-to-hydrogen efficiency of PV-EC-B system

Following general approach, the expression for STH in PV-EC-B system can be expressed as a ratio of total energy utilized in water splitting process E_{H2} to the total energy arrived at the PV cell E_{in} during one or multiple system operation cycles:

$$STH = \frac{E_{H2}}{E_{in}} = \frac{E_{H2l} + E_{H2d}}{E_{in}} \quad (6)$$

where E_{H2} is the sum of the energy directly supplied to the EC cell during the light period E_{H2l}, and the energy supplied to the EC cell from the battery in the dark E_{H2d}. These energies can be accessed via integration of the measured powers P_{H2l}, P_{H2d}, and P_{in} over the whole operation cycle $T = T_l + T_d$. The general approach with equation (6) has drawbacks for practical research. One drawback is the lack of time resolution – the estimate of *STH* in PV-EC-B system can be given only after one or several operation cycles. Another drawback is the indirect link between the IV characteristics of the PV, EC and the energies required to calculate *STH* with (6). For primary design and optimization of the PV-EC-B system it is desirable to estimate *STH* efficiency directly out of experimentally measured instantaneous values, e.g. currents. As we have shown in the previous subsections, in full charge utilization regime, total light current in the PV-EC-B system can be seen as a current in equivalent PV-EC system without special treatment of the storage phase. Thus, taking a single operation cycle and assuming full charge utilization we adopt the approach normally used to calculate *STH* in PV-EC systems to the system with battery. Typical *STH* expression for PV-EC system is:

$$STH = \frac{P_{H2}}{P_{in}} = \frac{\Delta E^{\circ}\eta_{FEC}I_{EC}}{P_{in}} \quad (7)$$

where P_{in} is the power of light impinging on the PV device and P_{H2} is a power consumed for hydrogen production, ΔE is the thermodynamic potential of water electrolysis ($\Delta E^{\circ} = 1.23$ V at 25 °C), η_{FEC} is faradaic efficiency, and I_{EC} is the current of the EC cell. To adopt the expression (7) to the PV-EC-B system the EC cell current I_{EC} is substituted by a sum of EC current I_{ECl} and battery currents multiplied by the battery Faradaic efficiency $\eta_{FB}I_{Bl}$:

$$STH^* = \frac{\Delta E\eta_{FEC}(I_{ECl} + \eta_{FB}I_{EBl})}{P_{in}} \quad (8)$$

The notation "*STH**" with asterisk is used to emphasize that battery charge utilization has to be considered in the case of PV-EC-B system. Using a combination of expressions (5) and (8) the expression for *STH** can be generalized to describe both modes of operation with full utilization and accumulation of charge:

$$STH^* = \begin{cases} \dfrac{\Delta E\eta_{FEC}(I_{ECl} + \eta_{FB}I_{Bl})}{P_{in}},\ Q_B < I_{ECd}T_d \\ \dfrac{\Delta E\eta_{FEC}(I_{ECl} + \eta_{FB}I_{ECd}T_d/T_l)}{P_{in}},\ Q_B > I_{ECd}T_d \end{cases} \quad (9)$$

For the best-case scenario with η_{FB} and η_{FEC} close to 100% [6,37,39] and full charge utilization expression (9) can be reduced to:

$$STH^* = \frac{\Delta EI_{ECBl}}{P_{in}} \quad (10)$$

which gives the maximum solar-to-hydrogen efficiency achievable with a given directly connected PV-EC-B system in full charge utilization regime. Note that expressions (7)–(10) do not include coupling factor and are valid for any power coupling. It means that even the "best-case-scenario" expression (10) does not describe the limit of the system. In order to estimate the maximum achievable *STH** the system has to be optimally coupled. To calculate maximal efficiency achieved by the PV-EC-B system and potential STH gain we need to return back to Fig. 3, where optimally coupled PV-EC and PV-EC-B systems are compared. It has been underlined that out of two optimally coupled systems PV-EC and PV-EC-B the same EC cell has lower overpotential in the case of PV-EC-B. Related power gain is graphically shown in Fig. 3 (a) with two colored rectangles. The rectangle "H_2 power EC only" represents the reference PV-EC system and the rectangle "H2 power gain" shows the gain potentially attained with use of the battery. This gain can be calculated using currents I_{EC} and I_{ECBl} indicated in Fig. 3 (a) with combination of expressions (7) and (10) as follows:

$$\Delta STH = STH^* - STH = \frac{\Delta E(I_{EC} - I_{ECBl})}{P_{in}} \quad (11)$$

Just as in expressions (7) to (10) the formula (11) generally apply to comparison of PV-EC-B and PV-EC system with any coupling. However, it is meaningful to compare optimally coupled systems to isolate the STH gain provided by the reduction of the kinetic losses in the EC cell.

3. Experimental PV-EC-B device

3.1. Experimental details

Experimental test of the PV-EC-B device function has been performed in the simplest configuration according to the circuit diagram shown in Fig. 1 (b). In order to provide acceptable voltage and power matching in the experimental PV-EC-B system the following components have been combined.

- PV device - a triple-junction solar cell [8] prepared in superstrate configuration (illuminated through the glass substrate). The top and middle sub-cells consist of amorphous silicon (a-Si:H) layers and the bottom cell consist of microcrystalline silicon (μc-Si:H). The silicon layers were deposited in a multi-chamber plasma-enhanced chemical vapor deposition system on fluorine doped tin oxide (SnO_2:F) coated glass substrate (type Asahi VU), the back contacts are made of sputtered aluminum doped zinc oxide and silver (ZnO:Al/Ag/ZnO:Al). The solar cell has area of 1 cm^2. Additional preparation details can be found elsewhere [8]. The solar cells were characterized by current–voltage (I–V) measurements at standard test conditions (100 mW cm^{-2}, 25 °C) using a double source (Class A) sun simulator reproducing AM1.5G standard spectrum. The cell has power conversion efficiency $\eta_{PV} = 11.3\%$, $FF = 67.9\%$, $V_{OC} = 2.25$ V, $J_{SC} = 7.4$ mA/cm^2.
- Electrochemical cell made of PEEK (Polyether ether ketone) has been filled with 1 M potassium hydroxide solution and Ni/Ni catalyst pair was used. Additional details on the catalyst preparation can be found elsewhere [11]. The catalyst area of 0.5 cm^2 size was defined by an O-ring sealing aperture. The electrochemical measurements where performed in two-electrode configuration at room temperature.
- Battery - Swagelok®-type Li-ion battery was prepared by using commercial LFP/C cathode and LTO anode. A glass fiber membrane soaked with LP30 electrolyte served as separator. This chemical composition has been chosen to provide theoretical voltage of about 1.90 V relevant for the operating voltage of the solar cell. The surface area of the LTO anode is 0.79 cm^2 with an active mass loading of 3.93 ± 0.3 mg, the surface area of LFP/C cathode is 1.13 cm^2. The battery is anode limited with theoretical total capacity of 0.68 ± 0.05mAh. Electrochemical characterization of the battery was performed using a VMP3 potentiostat (Bio-Logic, France) in a climate chamber MKF120 (Binder, Germany).

All three components PV, EC, and battery are of rather small scale with areas of 1 cm^2 and below. The term “system” used throughout the manuscript is related to the assembly of the elements but not the scale of the PV-EC or PV-EC-B devices.

The components of the PV-EC-B device were tested separately, and next, the PV-EC-B device was assembled according to the circuit diagram shown in Fig. 1 (b) and tested under one standard sun illumination with monitoring of the common voltage and individual currents I_{PV}, I_{ECl}, I_{Bl} over time. For the reverse operation, the PV-EC-B was operated in the dark with the PV cell disconnected. In the dark the EC cell was powered by the battery therefore EC current equals to battery discharge current in the dark, $I_{ECd} = I_{Bd}$.

3.2. Experimental results

Current-voltage characteristics of the PV cell, EC cell and battery are presented in Fig. 5 together with the common IV of the EC and the battery (EC-B). Battery IV is calculated with the model [26] calibrated with charge rate-overpotential data of the experimental battery. The voltage scale is magnified in Fig. 5 to present the relevant region with working points. The difference in light operation of both PV-EC and PV-EC-B systems is analyzed with correspondent combinations of IVs presented in the upper part of the figure Fig. 5 (a). The maximum power

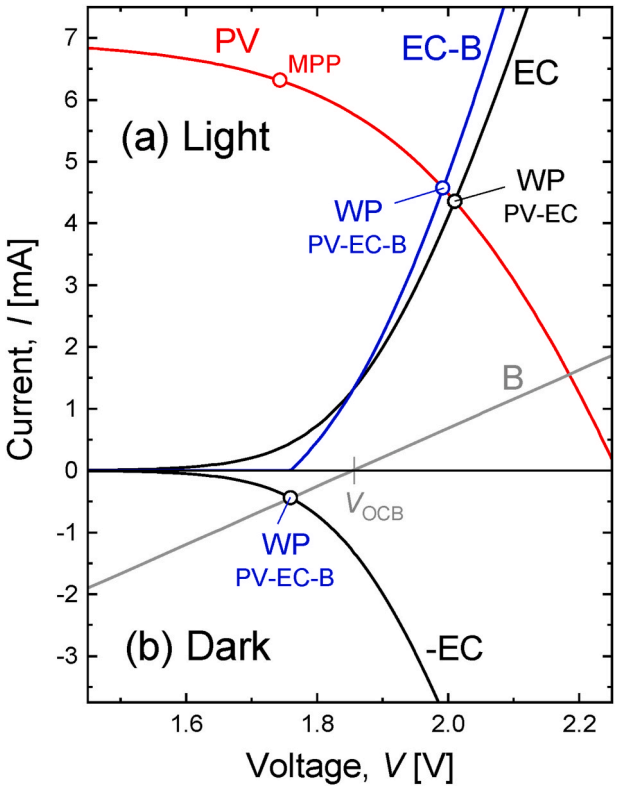

Fig. 5. Experimental current-voltage characteristics of PV cell (red), EC cell (black), calibrated simulation of battery IV (grey) and common IV of the EC and the battery (blue) denoted as EC-B. (a) Light period T_l: both PV-EC and PV-EC-B systems are active. Operating points of PV-EC, and PV-EC-B systems are indicated with open circles. (b) Dark period T_d: the PV-cell characteristic is absent and the battery is discharging via the EC cell. The battery current is changing direction and is presented as negative as well as the EC-cell IV. (For interpretation of the references to color in this figure legend, the reader is referred to the Web version of this article.)

point of the PV cell is shown with red open circle at the IV of the PV cell. The working point of the PV-EC system indicated with black open circle in Fig. 5 (a) is in the vicinity of MPP but does not coincide with it. This offset determines power coupling factor of $C = 0.8$ in PV-EC system.

When battery is connected in parallel to the EC cell the working point of the PV-EC-B system is defined by the intersection of the PV cell IV and common IV of EC and battery (blue curve EC-B) indicated by the blue open circle in Fig. 5 (a). It can be seen that the battery added to the PV-EC system has been charging during light period and shifted working point of the system towards MPP, changing power coupling to $C = 0.83$ in this case.

The case of dark operation of PV-EC-B system is presented in the lower part of the figure – Fig. 5 (b). Here the PV-cell is idle and disconnected (IV characteristic of PV cell is absent) and the battery is discharging via the EC cell. The battery current is changing direction and is presented as negative so EC IV is flipped in Fig. 5 (b) for consistency. In the dark period the working point of PV-EC-B system is determined by the intersection of the IV characteristics of the battery and EC cell as indicated by the black open circle. It can be seen in Fig. 5 (b) that the battery delivers stored energy to the EC cell for water splitting when PV is idle.

The behavior of the experimental PV-EC-B system has been studied on the time scale including light and dark periods. Fig. 6 presents voltage and current distribution between the EC cell and the battery for complete charge-discharge cycle. During the charging phase the solar cell provides the voltage of approx. 2.0 V across the EC cell and the battery while the current is distributed such that 3.8 mA flow through

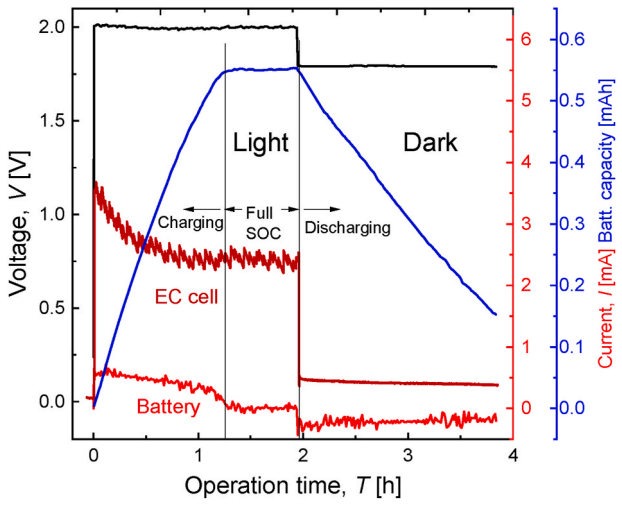

Fig. 6. EC-B voltage and current as well as the battery capacity as a function of the operation time for PV-EC-B system with Ni/Ni catalyst system. The noise in the current measurement is attributed to the formation and detachment of gas bubbles on the electrode surface [11].

the EC and 0.6 mA through the battery. The battery current decreases as charging progresses until full state of charge (SOC) is reached. At full SOC the battery capacity increases to 0.55 mAh (82% of the theoretical capacity). Then approximately for 40 min the battery current is at approx. zero and the EC cell takes the whole PV current. Once the light is turned off and solar cell is disconnected the discharge phase begins. During the discharge phase, the PV-EC-B reverts to EC-B and the battery drives the EC cell supplying current of −0.4 mA. The EC-B voltage drops to 1.75 V and battery linearly decreases as discharge progresses. The experiment was stopped at the battery capacity of approx. 0.15 mAh so as not to overdischarge the battery.

The results presented in Figs. 5 and 6 confirm the feasibility of the delayed utilization of some fraction of PV generated charge during dark periods in a PV-EC-B system without power management electronics. Note, the flat slope of the battery IV in Fig. 5. This is the result of insufficient battery capacity (0.68 mAh) for the charging rates in the experiment current range 1–3 mA leading to excessively high overpotentials. The only accessible batteries with voltage relevant for our experiment were lab scale coin cell devices with rather low capacity. For optimal operation of a realistic device the battery capacity has to be increased to reduce overpotentials. Nonetheless, even insufficiently scaled battery does improve performance of the PV-EC-B combination by picking up a part of the total current and shifting the working point closer to the MPP of the solar cell.

4. Optimization directions of the PV-EC-B system

Every element of PV-EC-B system can be improved in the course of system optimization. We focus on the battery and its key properties: open circuit voltage V_{OCB} and capacity. The duration of the discharge period is addressed as well, first in non-optimally coupled, and then in optimally coupled PV-EC-B system.

4.1. Role of the battery open circuit voltage

Considering combinations of IV characteristics of PV, EC and battery in any of the figures Figs. 2 and 3, or Fig. 5, it is easy to see that both light and dark working points depend on the position of the battery IV on the voltage scale – the battery open circuit voltage V_{OCB}. The battery open circuit voltage is a primary parameter for the power coupling, operation mode, and consequently efficiency of PV-EC-B system. To study the effect of V_{OCB} we combine experimental IVs of the PV and EC cells presented in Fig. 5, with simulated battery IV. The V_{OCB} is varied and characteristic voltages and currents are obtained numerically from the combinations of IVs (see e.g. Ref. [26]). Thereby we explore a range of V_{OCB} and our experiment results presented in Figs. 5 and 6 correspond to one of the V_{OCB} points. The results are presented in Fig. 7.

As presented in Fig. 7 (a) the sweep of V_{OCB} leads to shifts in the light and dark working point voltages of the PV-EC-B system determining all variations in currents, coupling factor, and *STH** presented in the graphs below. Currents of the system elements are presented in Fig. 7 (b). With increase of V_{OCB} the battery light current decreases, and the current balance shifts towards the light EC cell. At certain point V_{OCB} equalizes with the working point voltage of the PV-EC-B system V_{ECl}, and battery charging current I_{Bl} vanishes. If V_{OCB} increased further the battery would discharge even during light period. This would drain the battery and, on the long run eventually make it oscillate around lower voltage. In this work we consider behavior of the PV-EC-B system up to the point $V_{OCB} = V_{ECl}$ and not beyond. The average V_{OCB} observed in our experiment (Figs. 5 and 6) is represented by a vertical line denoted "experiment" in Fig. 7. The battery open circuit voltage in the experiment was below the light working point voltage V_{ECl} and therefore the battery was charging during light period. Total light current $I_{ECBl} = I_{Bl} + I_{ECl}$ in Fig. 7 (b) decreases with increase of V_{OCB} because the working point departs from the maximum power point towards V_{OC} of the PV-cell. This shift is illustrated by the coupling factor presented in Fig. 7 (c). Over the whole studied range, the PV-EC-B system was operating under non-optimal coupling with working point voltage above the MPP voltage of the PV-cell. Therefore, coupling factor C is higher at lower battery voltage and vice versa.

The dark working point voltage V_{ECd} and current I_{ECd} are shown in Fig. 7 (a) and Fig. 7 (b) respectively. At low V_{OCB} the dark working point voltage is low and the discharge current I_{ECd} is negligible. The discharge current I_{ECd} rises when the dark working point voltage reaches the onset of the exponential part of the EC cell IV characteristic. The battery charge currents I_{Bl} and I_{ECd} together with times T_l and T_d determine the charge balance in PV-EC-B system as described by expression (5). The charge balance in turn is a key factor for *STH** described by expression (9). As we can see in Fig. 7 (b) the current balance in the system depends on the battery open circuit voltage. Reduction of V_{OCB} shifts the balance towards battery charging – the current I_{Bl} increases but at the same time discharge current I_{ECd} declines, and the system tend to operate in charge accumulation mode.

Increase of the V_{OCB} shifts the balance towards the EC current I_{ECl} so the battery accumulates less charge and at the same time discharges at higher I_{ECd} (Fig. 7 (b)). Both factors bring the PV-EC-B system to the full charge utilization mode. From the prospective of a single operation cycle, charge accumulation mode is not optimal because charge is not fully utilized and is potentially lost. At the same time when the system is far in full charge utilization regime the effect of the battery on *STH** is reduced. The optimal operation regime of the PV-EC-B system is expected to be close to the transition between the full charge utilization and charge accumulation modes. For the calculations of *STH** we take $T_l = 8$ h as a top limit of peak sun hours [38] and consequently $T_d = 24$ h – $T_l = 16$ h. Using these T_l and T_d with currents presented in Fig. 7 (b) we calculate *STH** in PV-EC-B system according to the expression (9) and present in together with *STH* of the reference PV-EC system in Fig. 7 (d). It can be seen in Fig. 7 (d) that for a specific range of V_{OCB} the PV-EC-B system can outperform the system without battery even though the gain is relatively small, and is partially related to the coupling factor. The maximum of *STH** is at the point of critical charge utilization where $Q_B = I_{Ecd}T_d$. At lower V_{OCB}, *STH** sharply decreases due to insufficient charge utilization during the dark period T_d.

4.2. PV-EC-B with optimal coupling and high battery capacity

The results presented in Fig. 7 are calculated with experimental IVs of the PV and EC cells and experimentally calibrated model of the

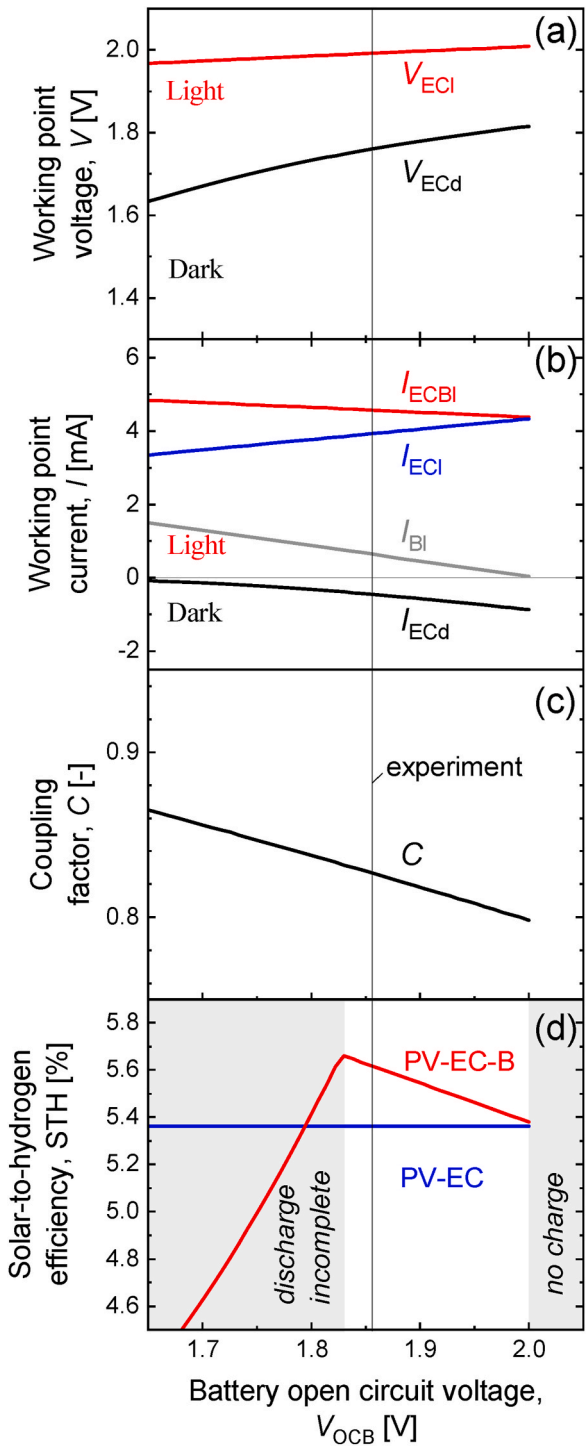

Fig. 7. Parameters of the PV-EC-B system as a function of the battery open circuit voltage V_{OCB}
(a) Working voltages of light and dark working points PV-EC-B system. (b) Light current of the battery I_{Bl}, light current of the EC cell I_{ECl}, total current of the light working point I_{ECBl}, and dark working point current I_{ECd}. (c) coupling factor in PV-EC-B system. (d) *STH** in PV-EC-B shown red against the *STH* in reference PV-EC system shown blue. Grey area on the left "discharge incomplete" indicates the range where PV-EC-B system is in the charge accumulation mode at $T_l = 8$ h. Grey area on the right indicates the range where V_{OCB} exceeds light working point voltage where battery is discharging even during the light phase. (For interpretation of the references to color in this figure legend, the reader is referred to the Web version of this article.)

battery IV where V_{OCB} is varied. In order to demonstrate potential gain in solar-to-hydrogen efficiency related to battery we repeat the calculations of *STH** with two modifications. First, the battery capacity has been increased to 35 mAh to ensure steep battery IV. Second, unlike in Fig. 7 no particular IV of the solar cell is used. For each value of V_{OCB} the working point of optimal coupling to PV device of same efficiency is found according to expression (3) for both PV-EC and PV-EC-B systems. The PV efficiency is constant and equals to the efficiency of the experimental cell $\eta_{PV} = 11.3\%$. This procedure can be seen as an application of ideal maximum power point tracker between PV cell and the load (EC or EC-B). in this way we can estimate how high the gain in STH can be with the use of the battery if both systems are based on the elements similar to the ones used in our experiment. In order to show the effect of charge-discharge time balance we performed calculations of *STH** for several durations of the light period, while keeping the same natural diurnal duty cycle $T_l + T_d = 24$ h. The results of *STH* calculated with (7) and STH* calculated with (9) are presented in Fig. 8 as a function of the battery open circuit voltage V_{OCB}.

It can be seen in Fig. 8 that the effect of V_{OCB} on *STH** is stronger in the case of 35 mAh battery as compared to the results in Fig. 7. At the same time the battery itself would operate in safer range of charge/discharge current. With using larger battery, the PV-EC-B system shows significantly higher *STH** in comparison to the reference PV-EC combination. The results in Fig. 8 are now free of the influence of coupling factor, so the gain in *STH** is entirely related to the gain in the EC cell efficiency facilitated by the battery. The maximum *STH** is observed in a specific range of V_{OCB} with the maximum shifting to lower voltages as the light time gets shorter. In natural pulsed day/night operation mode the battery spreads the PV energy over the whole operation cycle reducing specific power of the EC cell and related losses. The shorter light period is, the stronger this PV energy can be "stretched" on time scale. Consequently, the gain provided by the battery is higher for a duty cycle with short days of strong irradiance followed by long nights and vice versa. Since time is one of the key issues in estimation of the *STH** in the PV-EC-B system the exact value of the system efficiency can be given only for a specific duty cycle. The results presented in Fig. 8 can be used only as an approximation. We believe that solar-to-hydrogen efficiency

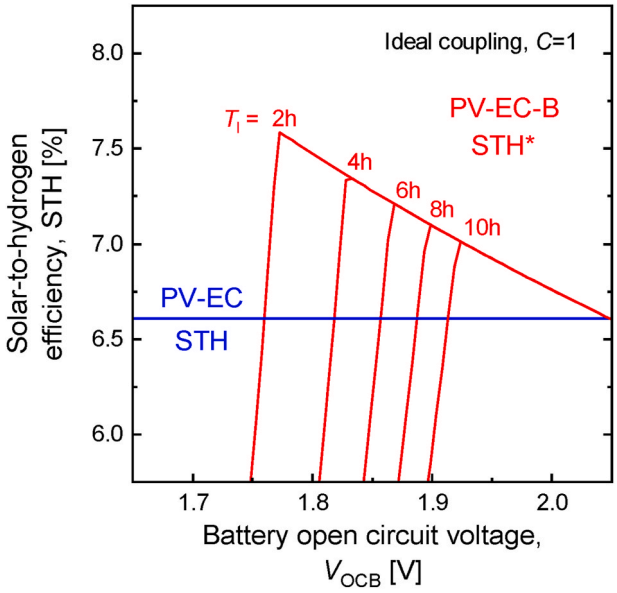

Fig. 8. Red lines: *STH** in optimally coupled PV-EC-B system as a function of V_{OCB} calculated for battery capacity of 35 mAh and different light periods indicated in hours the figure.
Blue line: reference *STH* calculated for the PV-EC system with optimal coupling. (For interpretation of the references to color in this figure legend, the reader is referred to the Web version of this article.)

gain of 5%–10% relative is achievable with properly scaled battery in PV-EC-B system.

The results of calculations in Fig. 8 are based on simplified duty cycle and constant battery voltage. Although modern commercial batteries in many cases exhibit flat charge/discharge characteristic [40–43], V_{OCB} is generally not constant if state of charge changes significantly. The drifts of V_{OCB} with state of charge will cause shifts of the battery IV on the voltage scale and therefore given PV-EC-B system would be represented by a range, rather than a point, in Fig. 7 or Fig. 8. Studies over multiple operation cycles are required to explore stability of operation, as well as the impact of the battery on the life of electrolyzers. The gain in efficiency facilitated by the battery will be also achieved if MPPT electronics [35] providing optimal coupling and for variety of electrochemical cells utilized under periodic irradiance. Finally, independent of the efficiency boost, properly chosen battery will smoothen out natural fluctuations of PV power which is expected to reduce related EC cell degradation.

5. Conclusions

In this work we included storage battery in directly interconnected photovoltaic-electrochemical water splitting system. We studied unaided operation of the PV-EC-B system with the battery connected in parallel to the EC cell, and analyzed solar-to-hydrogen efficiency (STH) in comparison to the reference PV-EC device. The PV-EC-B device was studied theoretically and experimentally with a simple test duty cycle of light period followed by the dark period. In the experiment a multijunction thin film Si PV cell was connected to an EC cell with Ni/Ni catalyst system and Li-ion battery.

Theoretical and experiment results demonstrate that battery connected in parallel to the EC cell can lead to a number of advantages: smoothen out the PV power fluctuations, facilitate power coupling, and even improve solar to hydrogen efficiency.

Simple parallel connection of PV, EC, and battery in PV-EC-B system is sufficient to provide partial storage of the PV energy and its further utilization for water splitting when PV is idle at night times. This facilitates smooth uninterrupted operation of the EC cell favorable for the stability of the electrolyzer.

Notably the spreading of the PV energy over the whole operation cycle reduces overpotential loss in the EC cell. Total overpotential loss in PV-EC-B system can be smaller than the loss in the reference PV-EC system. Therefore solar-to-hydrogen efficiency in PV-EC-B system can be higher compared to the reference PV-EC system. Consequently, efficiency of any PV-EC combination utilized under periodic irradiance can be improved with a battery of appropriate capacity and open circuit voltage.

Efficient operation of the PV-EC-B system relies in the first place on the proper choice of battery voltage and capacity which accounts for the durations of dark and light periods of the operation cycle. The battery open circuit voltage is a key parameter to maximize solar-to-hydrogen efficiency under given duty cycle. High battery capacities and duty cycles with short light periods followed by long dark periods are beneficial for STH in PV-EC-B system allowing utilization of battery charge at lower current and hence lower overpotential in the EC cell. The gain in STH of 5%–10% relative is expected for realistic duty cycles in PV-EC-B system as compared to equivalent reference PV-EC device.

Author contributions

Oleksandr Astakhov: investigation, data curation, formal analysis, software, visualization, writing – original draft, writing – review & editing.

Solomon Nwabueze Agbo: investigation, data curation, formal analysis, visualization, writing – original draft, writing – review & editing.

Katharina Welter: investigation, data curation, formal analysis writing – review & editing.

Vladimir Smirnov: investigation, formal analysis, writing – review & editing.

Uwe Rau: conceptualization, supervision, formal analysis.

Tsvetelina Merdzhanova: supervision, formal analysis, writing – review & editing.

CRediT authorship contribution statement

O. Astakhov: Investigation, Data curation, Formal analysis, Software, Visualization, Writing – original draft, Writing – review & editing. **S.N. Agbo:** Investigation, Data curation, Formal analysis, Visualization, Writing – original draft, Writing – review & editing. **K. Welter:** Investigation, Data curation, Formal analysis, Writing – review & editing. **V. Smirnov:** Investigation, Formal analysis, Writing – review & editing. **U. Rau:** Conceptualization, Supervision, Formal analysis. **T. Merdzhanova:** Supervision, Formal analysis, Writing – review & editing.

Declaration of competing interest

The authors declare that they have no known competing financial interests or personal relationships that could have appeared to influence the work reported in this paper.

Acknowledgments

Funding from H2020 project “A-leaf” grant agreement 732840, and JARA-Energy project ‘CO2 Valorization’ is acknowledged.

Hans Kungl, Shicheng Yu, Hermann Tempel for providing the battery samples.

Friedhelm Finger for critical and inspiring discussion.

References

[1] D.B. Manish Ram, Arman Aghahosseini, Ashish Gulagi, Solomon A. Oyewo, Michael Child, Upeksha Caldera, Kristina Sadovskaia, Javier Farfan, Larissa S.N. S. Barbosa, Mahdi Fasihi, Siavash Khalili, Bernhard Dalheimer, Georg Gruber, Thure Traber, Felix De Caluwe, Hans-Josef Fell, Christian Breyer, Global energy System based on 100% renewable energy – power, in: Heat, Transport and Desalination Sectors, *Study by Lappeenranta University of Technology and Energy Watch Group*, Lappeenranta University of Technology, Energy Watch Group, Lappeenranta, Berlin, 2019.

[2] T.L. Gibson, N.A. Kelly, Int. J. Hydrogen Energy 33 (2008) 5931–5940.

[3] N. Kelly, T. Gibson, D. Ouwerkerk, Int. J. Hydrogen Energy 33 (2008) 2747–2764.

[4] R.E. Clarke, S. Giddey, F.T. Ciacchi, S.P.S. Badwal, B. Paul, J. Andrews, Int. J. Hydrogen Energy 34 (2009) 2531–2542.

[5] T. Maeda, H. Ito, Y. Hasegawa, Z. Zhou, M. Ishida, Int. J. Hydrogen Energy 37 (2012) 4819–4828.

[6] C.R. Cox, J.Z. Lee, D.G. Nocera, T. Buonassisi, Proc. Natl. Acad. Sci. U. S. A. 111 (2014) 14057–14061.

[7] J. Rongé, T. Bosserez, L. Huguenin, M. Dumortier, S. Haussener, J.A. Martens, Oil Gas Sci. Technol. – Revue d’IFP Energies nouvelles 70 (2015) 863–876.

[8] F. Urbain, V. Smirnov, J.-P. Becker, A. Lambertz, F. Yang, J. Ziegler, B. Kaiser, W. Jaegermann, U. Rau, F. Finger, Energy Environ. Sci. 9 (2016) 145–154.

[9] J.-W. Schüttauf, M.A. Modestino, E. Chinello, D. Lambelet, A. Delfino, D. Dominé, A. Faes, M. Despeisse, J. Bailat, D. Psaltis, C. Moser, C. Ballif, J. Electrochem. Soc. 163 (2016) F1177–F1181.

[10] W.J. Chang, K.H. Lee, H. Ha, K. Jin, G. Kim, S.T. Hwang, H.M. Lee, S.W. Ahn, W. Yoon, H. Seo, J.S. Hong, Y.K. Go, J.I. Ha, K.T. Nam, ACS Omega 2 (2017) 1009–1018.

[11] K. Welter, N. Hamzelui, V. Smirnov, J.P. Becker, W. Jaegermann, F. Finger, J. Mater. Chem. 6 (2018) 15968–15976.

[12] J.H. Kim, D. Hansora, P. Sharma, J.W. Jang, J.S. Lee, Chem. Soc. Rev. 48 (2019) 1908–1971.

[13] V. Vega-Garita, L. Ramirez-Elizondo, N. Narayan, P. Bauer, Prog. Photovoltaics Res. Appl. 27 (2018) 346–370.

[14] G. Dennler, S. Bereznev, D. Fichou, K. Holl, D. Ilic, R. Koeppe, M. Krebs, A. Labouret, C. Lungenschmied, A. Marchenko, D. Meissner, E. Mellikov, J. Méot, A. Meyer, T. Meyer, H. Neugebauer, A. Öpik, N.S. Sariciftci, S. Taillemite, T. Wöhrle, Sol. Energy 81 (2007) 947–957.

[15] A. Gurung, Q. Qiao, Joule 2 (2018) 1217–1230.

[16] A. Hauch, A. Georg, U.O. Krašovec, B. Orel, J. Electrochem. Soc. 149 (2002) A1208–A1211.

[17] Y. Hu, Y. Bai, B. Luo, S. Wang, H. Hu, P. Chen, M. Lyu, J. Shapter, A. Rowan, L. Wang, Adv. Energy Mater. (2019) 1900872, 0.

[18] L.-C. Kin, z. liu, O. Astakhov, S.N. Agbo, H. Tempel, S. Yu, H. Kungl, R.-A. Eichel, U. Rau, T. Kirchartz, T. Merdzhanova, ACS Appl. Energy Mater. (2019), https://doi.org/10.1021/acsaem.9b01672.
[19] G. Merei, J. Moshövel, D. Magnor, D.U. Sauer, Appl. Energy 168 (2016) 171–178.
[20] J. Koponen, A. Kosonen, V. Ruuskanen, K. Huoman, M. Niemelä, J. Ahola, Int. J. Hydrogen Energy 42 (2017) 29648–29660.
[21] J.D. Maclay, J. Brouwer, G.S. Samuelsen, Int. J. Hydrogen Energy 36 (2011) 12130–12140.
[22] J.P. Becker, B. Turan, V. Smirnov, K. Welter, F. Urbain, J. Wolff, S. Haas, F. Finger, J. Mater. Chem. 5 (2017) 4818–4826.
[23] S.N. Agbo, T. Merdzhanova, S.C. Yu, H. Tempel, H. Kungl, R.A. Eichel, U. Rau, O. Astakhov, J. Power Sources 327 (2016) 340–344.
[24] S.N. Agbo, T. Merdzhanova, S.C. Yu, H. Tempel, H. Kungl, R.A. Eichel, U. Rau, O. Astakhov, Phys. Status Solidi 213 (2016) 1926–1931.
[25] F. Sandbaumhuter, S.N. Agbo, C.L. Tsai, O. Astakhov, S. Uhlenbruck, U. Rau, T. Merdzhanova, J. Power Sources 365 (2017) 303–307.
[26] O. Astakhov, T. Merdzhanova, L.-C. Kin, U. Rau, Sol. Energy 206 (2020) 732–740.
[27] M.T. Winkler, C.R. Cox, D.G. Nocera, T. Buonassisi, Proc. Natl. Acad. Sci. Unit. States Am. 110 (2013) E1076.
[28] F. Urbain, V. Smirnov, J.-P. Becker, A. Lambertz, U. Rau, F. Finger, Sol. Energy Mater. Sol. Cells 145 (2016) 142–147.
[29] P. Reale, A. Fernicola, B. Scrosati, J. Power Sources 194 (2009) 182–189.
[30] Y. Honda, S. Muto, K. Tatsumi, H. Kondo, K. Horibuchi, T. Kobayashi, T. Sasaki, J. Power Sources 291 (2015) 85–94.
[31] J. Bonse, S. Hohm, S.V. Kirner, A. Rosenfeld, J. Kruger, IEEE J. Sel. Top. Quant. Electron. 23 (2017).
[32] Q. Zhang, T. Li, J. Luo, B. Liu, J. Liang, N. Wang, X. Kong, B. Li, C. Wei, Y. Zhao, X. Zhang, J. Mater. Chem. 6 (2018) 811–816.
[33] S. Hu, C. Xiang, S. Haussener, A.D. Berger, N.S. Lewis, Energy Environ. Sci. 6 (2013).
[34] J.-P. Becker, F. Urbain, V. Smirnov, U. Rau, J. Ziegler, B. Kaiser, W. Jaegermann, F. Finger, Phys. Status Solidi 213 (2016) 1738–1746.
[35] J.-A. Jiang, Y.-L. Su, K.-C. Kuo, C.-H. Wang, M.-S. Liao, J.-C. Wang, C.-K. Huang, C.-Y. Chou, C.-H. Lee, J.-C. Shieh, Renew. Sustain. Energy Rev. 69 (2017) 1113–1128.
[36] F. Saidani, F.X. Hutter, R.-G. Scurtu, W. Braunwarth, J.N. Burghartz, Adv. Radio. Sci. 15 (2017) 83–91.
[37] B.D. Adams, J. Zheng, X. Ren, W. Xu, J.-G. Zhang, Adv. Energy Mater. 8 (2018).
[38] U. Y. Tito, L. Quispe-Huaman and O. A. Vilca-Huayta, 2020.
[39] J. Brillet, J.-H. Yum, M. Cornuz, T. Hisatomi, R. Solarska, J. Augustynski, M. Graetzel, K. Sivula, Nat. Photonics 6 (2012) 824–828.
[40] X. Sun, P.V. Radovanovic, B. Cui, New J. Chem. 39 (2015) 38–63.
[41] M.A. Roscher, O. Bohlen, J. Vetter, Int. J. Electrochem. 2011 (2011) 1–6.
[42] E. Hosono, H. Matsuda, I. Honma, M. Ichihara, H. Zhou, J. Electrochem. Soc. (2007) 154.
[43] C.M. Julien, A. Mauger, Ionics 19 (2013) 951–988.